

## RESEARCH ARTICLE

Molecular insight into *Aspergillus oryzae*  $\beta$ -mannanase interacting with mannotriose revealed by molecular dynamic simulation studyUttam Kumar Jana<sup>1☯✉</sup>, Gagandeep Singh<sup>2,3☯</sup>, Hemant Soni<sup>2</sup>, Brett Pletschke<sup>4\*</sup>, Naveen Kango<sup>1\*</sup>

**1** Department of Microbiology, Dr. Harisingh Gour Vishwavidyalaya (A Central University), Sagar, Madhya Pradesh, India, **2** Central Ayurveda Research Institute, Jhansi, Uttar Pradesh, India, **3** Indian Institute of Technology, Delhi, India, **4** Enzyme Science Programme (ESP), Department of Biochemistry and Microbiology, Rhodes University, Makhanda, South Africa

☯ These authors contributed equally to this work.

✉ Current address: Crystallography & Molecular Biology Division, Saha Institute of Nuclear Physics, Kolkata, West Bengal, India

\* [nkango@gmail.com](mailto:nkango@gmail.com) (NK); [b.pletschke@ru.ac.za](mailto:b.pletschke@ru.ac.za) (BP)



## OPEN ACCESS

**Citation:** Jana UK, Singh G, Soni H, Pletschke B, Kango N (2022) Molecular insight into *Aspergillus oryzae*  $\beta$ -mannanase interacting with mannotriose revealed by molecular dynamic simulation study. PLoS ONE 17(9): e0268333. <https://doi.org/10.1371/journal.pone.0268333>

**Editor:** Sabato D'Auria, Consiglio Nazionale delle Ricerche, ITALY

**Received:** November 29, 2021

**Accepted:** April 28, 2022

**Published:** September 16, 2022

**Peer Review History:** PLOS recognizes the benefits of transparency in the peer review process; therefore, we enable the publication of all of the content of peer review and author responses alongside final, published articles. The editorial history of this article is available here: <https://doi.org/10.1371/journal.pone.0268333>

**Copyright:** © 2022 Jana et al. This is an open access article distributed under the terms of the [Creative Commons Attribution License](https://creativecommons.org/licenses/by/4.0/), which permits unrestricted use, distribution, and reproduction in any medium, provided the original author and source are credited.

**Data Availability Statement:** All relevant data within the article and uploaded to Mendelay at DOI: [10.17632/k2s39zw92c.1](https://doi.org/10.17632/k2s39zw92c.1) (<https://data.mendeley.com/datasets/k2s39zw92c/1>).

## Abstract

Fungal  $\beta$ -mannanases hydrolyze  $\beta$ -1, 4-glycosidic bonds of mannans and find application in the generation of mannose and prebiotic manno oligosaccharides (MOS). Previously, a MOS generating  $\beta$ -mannanase from *Aspergillus oryzae* MTCC 1846 ( $\beta$ ManAo) was characterized and its structural and functional properties were unraveled through homology modeling and molecular dynamics in this study. The  $\beta$ ManAo model was validated with 92.9% and 6.5% of the residues found to be distributed in the most favorable and allowed regions of the Ramachandran plot. Glu244 was found to play a key role in the interaction with mannotriose, indicating conserved amino acids for the catalytic reaction. A detailed metadynamic analysis of the principal components revealed the presence of an  $\alpha_8$ -helix in the C-terminus which was very flexible in nature and energy landscapes suggested high conformation sub-states and the complex dynamic behavior of the protein. The binding of the M3 substrate stabilized the  $\beta$ -mannanase and resulted in a reduction in the intermediate conformational sub-states evident from the free energy landscapes. The active site of the  $\beta$ -mannanase is mostly hydrophilic in nature which is accordance with our results, where the major contribution in the binding energy of the substrate with the active site is from electrostatic interactions. Define Secondary Structure of Proteins (DSSP) analysis revealed a major transition of the protein from helix to  $\beta$ -turn for binding with the mannotriose. The molecular dynamics of the  $\beta$ ManAo–mannotriose model, and the role and interactions of catalytic residues with ligand were also described. The substrate binding pocket of  $\beta$ ManAo was found to be highly dynamic and showed large, concerted movements. The outcomes of the present study can be exploited in further understanding the structural properties and functional dynamics of  $\beta$ ManAo.

**Funding:** The author(s) received no specific funding for this work.

**Competing interests:** The authors have declared that no competing interests exist.

## 1. Introduction

Prebiotic oligosaccharides are non-digestible carbohydrates that confer numerous health benefits and have become a recent center of attention. These compounds are emerging as an alternative to antibiotics and may play a crucial role in mitigating the emergence of anti-microbial resistance in the host [1, 2]. Different oligosaccharides available in the market are obtained either by extraction from plants or derived by enzymatic hydrolysis of various polysaccharides. Manno oligosaccharides (MOS) are short-chains of mannose obtained after enzymatic hydrolysis of mannans using endo- $\beta$ -(1, 4)-mannanase (EC 3.2.1.78). Mannan-rich substrates like guar galactomannan (GG), locust bean galactomannan (LBG) and konjac glucomannan are the major sources exploited for deriving MOS [3]. The endo- $\beta$ -(1, 4)-mannanase is capable of producing different oligomers of varying degree of polymerization (DP) based on the affinity and mechanism of the enzyme [4]. Like mannans, MOS also contain (1, 4)- $\beta$ -linked D-mannopyranosyl units and are comprised of mannobiose (M2), mannotriose (M3), maltotetraose (M4), mannopentose (M5), etc.

$\beta$ -mannanases find diverse applications in the food and feed, biofuel, oil, coffee, paper and pulp, textile industries, etc. [5]. According to the CAZy database, the majority of  $\beta$ -mannanases belong to 5, 26 and 113 glycosyl hydrolase (GH) families [6]. The GH5 family is a complex family with different hydrolases, including  $\beta$ -mannanases which have a  $(\beta/\alpha)_8$  TIM barrel structure and contain a -1 sub-site of the enzyme as sugar-binding site [7]. Although mannanases with similar catalytic activities are found in different microorganisms, their abilities to bind to oligosaccharides vary, especially in the case of fungi, as these can degrade diverse hardwoods [8]. The filamentous fungus, *Aspergillus oryzae*, enjoys a GRAS status by the USA Food and Drug Administration [9]. It is employed for various purposes, especially in the production of fermented foods and various industrial enzymes (e.g.  $\alpha$ -amylase). *A. oryzae* produces a vast range of extracellular enzymes in both solid-state and liquid cultures, with glycosyl hydrolases being the predominant enzymes. In this context, we have reported the production and characterization of a MOS generating  $\beta$ -mannanase from *A. oryzae* MTCC 1846 [10]. The  $\beta$ -mannanase showed a high rate of conversion of mannan into MOS and the oligosaccharides were shown to confer prebiotic effects [11].

Homology modeling is a computational structure prediction tool that estimates the 3D structure of a desired protein and compares it with a similar template. It is a highly precise structural prediction method that requires less time. Thus, it is very effective for the screening of different drugs and ligands based on the model [12]. Molecular docking is used to study the interaction between a ligand and a protein at the atomic residue level. The interaction reveals the biophysical and biochemical behavior of the ligand as well as the binding site of the protein. The docking process consists of ligand conformation prediction and its position and orientation within the active site (s) of the enzyme and also helps understand binding affinity of the docked molecule [13, 14]. MD simulation has been used for the analysis of conformational rearrangements of molecules and it assists in understanding the macromolecular structure-to-function relationships between the protein and ligand complex in different environments. MD simulation represents a system with several atoms, including the protein in environments mimicking a natural one [15].

In the present study, homology modeling, molecular docking and molecular dynamics simulations of  $\beta$ -mannanase from *A. oryzae* were performed, and interaction with mannotriose was reported. The structural and the biophysical properties of the  $\beta$ -mannanase were also evaluated.

## 2. Materials and methods

### 2.1 Protein sequence retrieval and domain identification

The three-dimensional (3D) structure of  $\beta$ -mannanase from *A. oryzae* is not currently available in the protein data bank server. For this reason, the amino acid sequence of mannanase from *A. oryzae* ( $\beta$ ManAo) was retrieved from the UniProt (<http://www.uniprot.org/>) database (Uniprot ID: Q2TXJ2). The prediction of different conserved domains present in  $\beta$ ManAo was evaluated using Pfam (<http://pfam.xfam.org/>), InterProScan (<https://www.ebi.ac.uk/interpro/>) and the Conserved Domain Database (CDD) (<https://www.ncbi.nlm.nih.gov/cdd/>) database servers. The EMBL-EBI Enzyme portal (<https://www.ebi.ac.uk/enzymeportal/>) was used to predict the substrate binding site and active site residues of the modelled  $\beta$ ManAo from *A. oryzae*.

### 2.2 System preparation, refinement and validation

A suitable template for homology modeling of  $\beta$ ManAo was searched for using the pBLAST suite in the Protein Data Bank (PDB) database. Results were based on the highest alignment score percentage of identity and similarity and the lowest E-value, and the best homologous structure template was retrieved. The homology modeling of  $\beta$ ManAo was executed using a Swiss model homology modeling server [16]. Energy minimization and optimization of hydrogen bonding network were carried out by 3Drefine [17]. Protein secondary structures were determined by SOPMA [18]. The percentage of identity and similarity, superimpose score, and calculation of global root mean square deviation (RMSD) between the target and template were calculated by the SuperPose server [19]. The stereo-chemical quality of the model was evaluated using a Ramachandran plot by analyzing residue-by-residue and overall structure geometry by Procheck [20]. Comparison between homology modeling, X-ray and NMR structure was predicted by ProSA and the Z-score of the model was also calculated by the web-server [21]. ERRAT was used for the statistical analysis of various atom types and non-bonded interactions of the refined model and also for plotting the error function value versus position of a 9-residue sliding window [22]. The compatibility of the atomic model with amino acid sequence by calculating a structural class of different location and environment (polar, non-polar, loop, alpha, beta, etc.) was predicted by Verify 3D [23]. The secondary and super secondary structure of the model was evaluated by Stride [24]. QMEAN was used for predicting theoretical model Z-score in comparison to a non-redundant set of PDB structures [25].

### 2.3 *In silico* physico-chemical characterization of $\beta$ ManAo

Different physicochemical characters such as molecular weight, number of positive and negatively charged amino acids, extinction coefficient, theoretical isoelectric point, aliphatic index, instability index and grand average hydropathicity (GRAVY) of  $\beta$ ManAo were predicted by ExPASy's ProtParam web server tool (<http://web.expasy.org/protparam/>). Secondary structure, solvent accessibility, and different ontology studies such as molecular function, cellular components, and biological process were predicted by the Predict Protein server (<https://predictprotein.org/>).

### 2.4 Intra-atomic interaction analysis of $\beta$ ManAo

The non-covalent intra-molecular interaction including H-bonds, ionic bonds, disulfide bonds,  $\pi$ -cation, and  $\pi$ - $\pi$  stacking bonds of  $\beta$ ManAo at the atomic level was visualized using the Residue Interaction Network Generator (RING) web server and Arpeggio web server [26, 27]. The salt bridges in the protein structure were analyzed by the ESBRI web server [28].

## 2.5 Ligand preparation

The interaction between  $\beta$ ManAo with mannotriose was investigated using the molecular docking method. The topological properties (including the surface pockets and interior cavities of the homology model) were predicted by CASTp 3.0, which exhibited the negative volumes of different binding pockets and gave secondary structure, functional sites, variant sites, and other annotations of protein residues of the enzyme [29]. 3D structure of mannotriose was retrieved in SDF format from the PubChem database (M3, PubChem ID: 3010288). The energy minimization of mannotriose was performed using the minimize structure tools, where the parameters like steepest descent steps (100), steepest descent step size (0.02 Å), conjugate gradient steps (10), conjugate gradient step size (0.02 Å) and update interval (10) were set for the minimization step. The minimizations of standard residues were performed using the AMBER ff14SB force field and other residues were executed using the Gasteiger force field.

## 2.6 Molecular docking

The molecular docking between M3 and  $\beta$ ManAo was executed using AutoDock 4.2 [30]. The grid box was generated by AutoGrid and selected 3D coordinates in x, y, z-dimensions, where the active site of the enzyme as well as a large portion of adjoining surface was covered. After completing the docking process, nine probable docking structures were generated and the best combination was evaluated on the basis of minimum binding energy (Kcal/mol), number of hydrogen bonds, docking score, and other weak interactions. Results were visualized using Discovery Studio Software. The absolute binding affinity of  $\beta$ ManAo-M3 complex was predicted by  $K_{DEEP}$  [31].

## 2.7 Molecular dynamics simulation

In order to assess the stability of  $\beta$ ManAo structure, an all-atom molecular dynamic simulation of  $\beta$ ManAo and  $\beta$ ManAo-M3 was run using LiGRO [32], a GUI based software that prepares the necessary files required for MD simulations using GROMACS 5.1.5 [33]. The protein was solvated in a cubic box filled with TIP3P water molecules such that the distance between two periodic images was 2 nm. The amber99sb forcefield was used for protein while the topology for the M3 substrate was generated using an integrated ACPYPE module of LiGRO with General Amber Force Field (GAFF) and bcc charges [34]. The system was neutralized by adding 150 mM NaCl. In order to remove the steric clashes, the system was energy minimized using 5000 steps of steepest descent followed by a conjugate gradient with a tolerance of 10.0 kJ/mol/nm. The system was subjected to equilibration under NVT and NPT ensembles for 1 ns each at 310.15 K and 1 bar, using a modified Berendsen thermostat and Parrinello-Rahman barostat, respectively. The verlet cutoff-scheme was used for neighbor searching with short range electrostatic and van der Waals energy cutoff values of 1.4 nm. The molecular dynamic production simulation of 100 ns under NPT ensemble was run on the high-performance computing cluster at the Indian Institute of Technology, Delhi (HPC-IITD). A PME method and LINCS algorithm were applied to correct for the long-range electrostatic interactions and to constrain the covalent bonds. A time step of 2 fs was used while the frames were updated after every 500 steps. The trajectory was visualized using VMD and Chimera and standard GROMACS tools were used to analyze the trajectory.

**2.7.1 Geometrical properties.** Different geometrical parameters such as the radius of gyration (RG), number of hydrogen bonds (NHB), root mean square deviation (RMSD), root mean square fluctuation (RMSF), and energy components such as entropy, Gibbs free energy of binding of protein and protein-ligand complex were calculated with respective programs

using GROMACS tools. The substrate binding pocket flexibility and dynamics were analyzed using TRAPP webserver [35].

**2.7.2 Principal component analysis.** Principal component analysis (PCA) is a technique to increase the interpretability of large datasets by reducing the complexity of the data and lowering the information loss from the dataset. PCA was implemented with the new uncorrelated variables using a variance/covariance matrix generated from MD trajectories. A covariance matrix was obtained from the atomic fluctuation after separating the rotational and translational movement and it was represented by the simple linear transformation in Cartesian coordinate space. Further, diagonalization of the matrix ( $C_{ij}$ ) in PCA was obtained through an orthogonal matrix by computing on the basis of Eq (1).

$$C_{ij} = V\Lambda V^T \quad (1)$$

where,  $\Lambda$  = eigenvalues as diagonal entries,  $V$  = represents the related eigenvectors and  $T$  = orthogonal coordinate transformation matrix. The PCA plots for the  $\beta$ ManAo and  $\beta$ ManAo-M3 models were generated using the Geo-Measures [36] plugin in PyMOL employing the first two most populated principal components (PC1 and PC2).

**2.7.3 Free energy landscape analysis.** Free energy landscapes of any system explain all the conformational entities of a molecule and their roles in interacting with other molecules with respect to the spatial position, and play a key role in deciphering their respective free energy levels. The free energy landscapes (FELs) of the  $\beta$ ManAo and  $\beta$ ManAo-M3 models were constructed using the Geo-Measures tool employing the trajectory RG by RMSD values. Geo-Measures were employed by using the g\_sham tool of the GROMACS package to generate the FEL ([https://manual.gromacs.org/archive/4.6.1/online/g\\_sham.html](https://manual.gromacs.org/archive/4.6.1/online/g_sham.html)). The stable energetic conformations were marked in blue, while the less stable conformations were marked in red regions.

**2.7.4 Binding free energy calculations using MMGBSA methods.** The MMGBSA module of the gmx\_MMPBSA tool was used to calculate the binding energy  $\Delta G$  from the last 100 frames from the 90-100ns interval of the trajectory [37]. The GB method used was igb = 2 with internal and external dielectric constants of 1 and 80, respectively, being applied. The entropic contributions were estimated by normal mode analysis (NMA). The estimated  $\Delta G$  is given by Eq (3),

$$\Delta G = \Delta H - T\Delta S = \Delta G_{\text{gas}} + \Delta G_{\text{solv}} - T\Delta S \quad (2)$$

where,  $\Delta G_{\text{gas}} = \text{EEL} + \text{VDWAALS}$ , represents the total gas phase energy consisting of electrostatic and Van der Waals interaction energies,  $\Delta G_{\text{solv}} = \text{EGB} + \text{ESURF}$ , are the polar and non-polar solvation free energies and  $T\Delta S$  corresponds to the change in conformational entropy on binding.

**2.7.5 Define Secondary Structure of Proteins (DSSP) analysis.** The secondary structural changes in the protein with respect to the frames in the trajectory of  $\beta$ ManAo and  $\beta$ ManAo-M3 were measured by DSSP [38]. The secondary structure was labeled as 'H' for helix, 'E' for strands and 'C' for the coils.

## 3. Results and discussions

### 3.1 System preparation, refinement and validation

The 3D structure of  $\beta$ ManAo had the maximum homology with the chain A of  $\beta$ -mannanase from *A. niger* with a 70.93% identity among their amino acids and belonged to the GH5 glycosyl hydrolase family (Fig 1A). The total score, query coverage, and E-value between the two



chain A of 3WH9 and pair-wise alignment are presented in Fig 1D. Similar to the NCBI protein BLAST, the identity percentage was 70%, whereas the similarity score was 83%. The base-pair wise structure alignment is shown in Fig 1E. Protein Structure Analysis (Pro-SA) is a useful tool for the refinement and validation of an experimental structure. The main parameter for Pro-SA is the Z-score which evaluates the overall structure quality, as well as provides a measure of the total energy deviation of the structure with the help of energy deviation based on random conformation. For this reason, the value of the Z-score of the protein model outside the region and the positive value of the energy plot is referred as problematic and erroneous [21]. Here, the Z-value of the X-ray structures estimated for  $\beta$ ManAo was -8.72 (Fig 1F) and the maximum sequences were in the negative energy mode (Fig 1F), which corresponded to the correct model. In addition, the Z-score of the predicted model was calculated by a normalized QMEAN score of  $0.5 < \text{score} < 1$ , when compared with a non-redundant set of PDB structures, which suggested the appropriateness of the model with high quality (Fig 2A).

The Ramachandran plot for  $\beta$ ManAo obtained from Procheck showed that all the amino acids of the predicted model make a favorable region, where 92.9% were in the most favored regions, 6.5% in the additional allowed regions, and 0.7% in the generously allowed regions. No residues were present in the disallowed regions and R-factor was not greater than 20%, which again indicated a good quality model (Fig 2B). Furthermore, the G-factor of the model

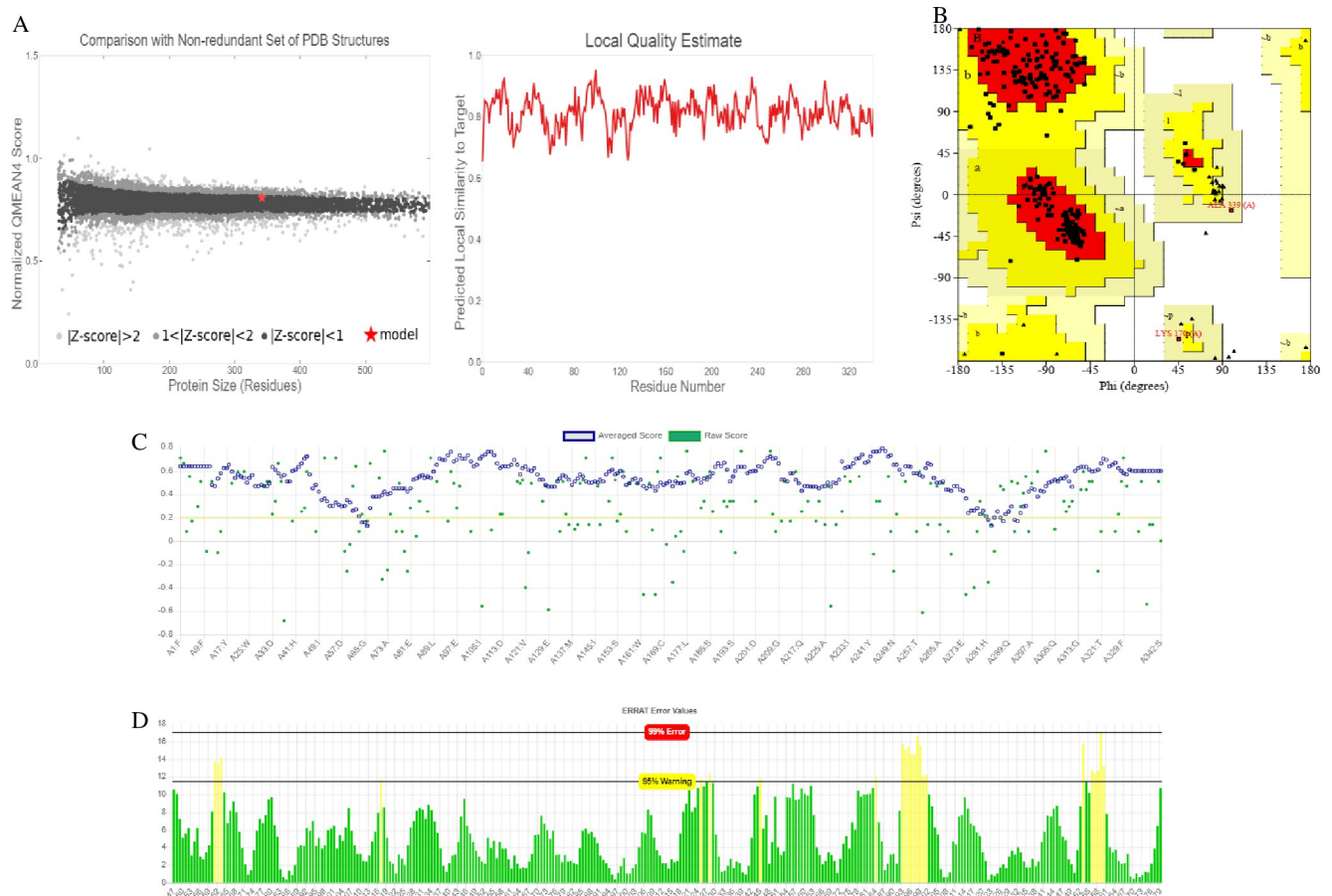


**Fig 2. Validation of the predicted  $\beta$ ManAo model.** (A) QMEAN score of the predicted model and local quality estimation of the model, (B) Ramachandran plot of  $\beta$ ManAo by Procheck indicated that all the amino acids residues are falling in the allowed region, (C) Assessment of 3D model of  $\beta$ ManAo by Verify 3D and (D) Assessment of non-bonding interaction of different atoms by ERRAT.

<https://doi.org/10.1371/journal.pone.0268333.g002>

was -0.58, which was low and satisfactory, as the higher negative value of the G-factor refer to the low-probability conformation with amino acid residues of the model falling in the disallowed regions of the Ramachandran plot. The 3D model assessment through Verify 3D resulted in 97.66% of the residues with an average 3D - 1D score  $> 0.2$ . Fig 2C depicts the plot of 3D-1D score of amino acids of  $\beta$ ManAo. ERRAT analysis was found to be 93.1138, which indicated a recommended statistical value for non-bonded interactions between different atom types and value of error function vs. position of a 9-residue a sliding window of the refined model (Fig 2D). Therefore, after the quality and refinement assessment of  $\beta$ ManAo, it was concluded that the predicted model of the  $\beta$ -mannanase from *A. oryzae* showed stereochemical stability and can be successfully used for further analysis.

### 3.2 Physico-chemical properties of $\beta$ ManAo

The pI of  $\beta$ ManAo was computed as 4.69, indicating the acidic nature of  $\beta$ ManAo. The extinction coefficient of the predicted  $\beta$ ManAo was  $88155 \text{ M}^{-1} \text{ cm}^{-1}$  at 280 nm, which indicated the hydrophobic nature of the enzyme due to the presence of 54.92% non-polar amino acids.  $\beta$ ManAo had two disulfide (S-S) bonds, which provided stability to the 3D structure as well as assisted in redox activity. The presence of disulfide bonds also indicated the secretory nature of the protein [39]. The instability index (II) of  $\beta$ ManAo was computed to be 21.55, which showed that the protein was highly stable under the suggested *in vitro* conditions (Table 1).

Similarly,  $\beta$ -glucosidase from *Trichoderma* sp. had an instability index of 31.25 [40].  $\beta$ ManAo had a higher aliphatic index of 70.54, which is the reason for its activity over a wide temperature range, while a negative value of GRAVY (-0.28) indicated its more favorable aqueous interactions. As suggested by the model,  $\beta$ ManAo had a high content of alanine (8.3%), glycine (10.1%) and serine (10.1%) amino acids.

### 3.3 Domain and substrate binding pocket analysis of $\beta$ ManAo

Analysis of different domains through Pfam, InterProScan and Conserved Domain Database (CDD) revealed that the protein had two conserved domains, such as Signal peptide (1–21 AA) and the main glycosyl hydrolase (GH5) ranging from 51 to 378 AA (Fig 1A). The GH5 domain displayed close homology with the chain A of 3WH9 (PDB ID), which was found to be an endo- $\beta$ -1, 4- mannanase from *Aspergillus niger*. The substrate binding and active site residues of  $\beta$ ManAo were predicted by EMBL-EBI Enzyme portal. The predicted substrate binding residues include Trp95, Asn207, Tyr 283 and Trp346 (on sharing similarity with  $\beta$ -mannanase of *Cryptopygus antarcticus*, Uniport: B4XC07) and the active site residues include Glu208 (Proton donor) and Glu316 (Nucleophile) (on sharing similarity with  $\beta$ -mannanase

**Table 1. Predicted physico-chemical characteristics of  $\beta$ ManAo through ExPASy's protparam.**

Protein ID (Uniprot)	Q2TXJ2
Sequence length (No. of AA)	386
Molecular weight	41906 Da
pI	4.69
Total number of negatively charged residues (ASP + GLU)	42
Total number of positively charged residues (ARG + LYS)	24
Extinction coefficient	87780
Instability index (II)	21.55
Aliphatic index	70.54
GRAVY	-0.288

<https://doi.org/10.1371/journal.pone.0268333.t001>

from *Trichoderma reesei*, Uniprot: Q99036). These predictive results are in accordance with our docking results where the M3 molecule is interacting with the predicted substrate binding and active site residues.

### 3.4 Intra-atomic interactions

Among all the intramolecular actions, hydrophobic interactions and hydrogen bonds were found to be the major reason for the stability of  $\beta$ ManAo (Fig 3).

A total 1072 hydrophobic interactions and 444 H-bonds were present.  $\beta$ ManAo had more charged polar amino acids on the surface while non-polar side chains were buried, which made a favorable contribution to protein stability by removing the non-polar side chains from water and enhancing the London dispersion forces that result in the tight packing of protein from the interior side [41]. H-bonds are not only involved in protein-ligand interactions, but are also crucial for the conformational stability of a protein for optimum physical properties [42]. Asp, Arg, and Glu were the main amino acids involved in the ionic interactions. The endo- $\beta$ -mannanase from *Arabidopsis thaliana* formed two ionic bonds with mannose at Glu252 [43]. Ionic interactions increase the thermo-stability of the enzymes, while ionic-pair networks help enzymes withstand the local environment [44]. As discussed earlier, the enzyme had two disulfide bonds at the positions Cys373-Cys324 and Cys312-Cys305 (Fig 3). The  $\beta$ -1,

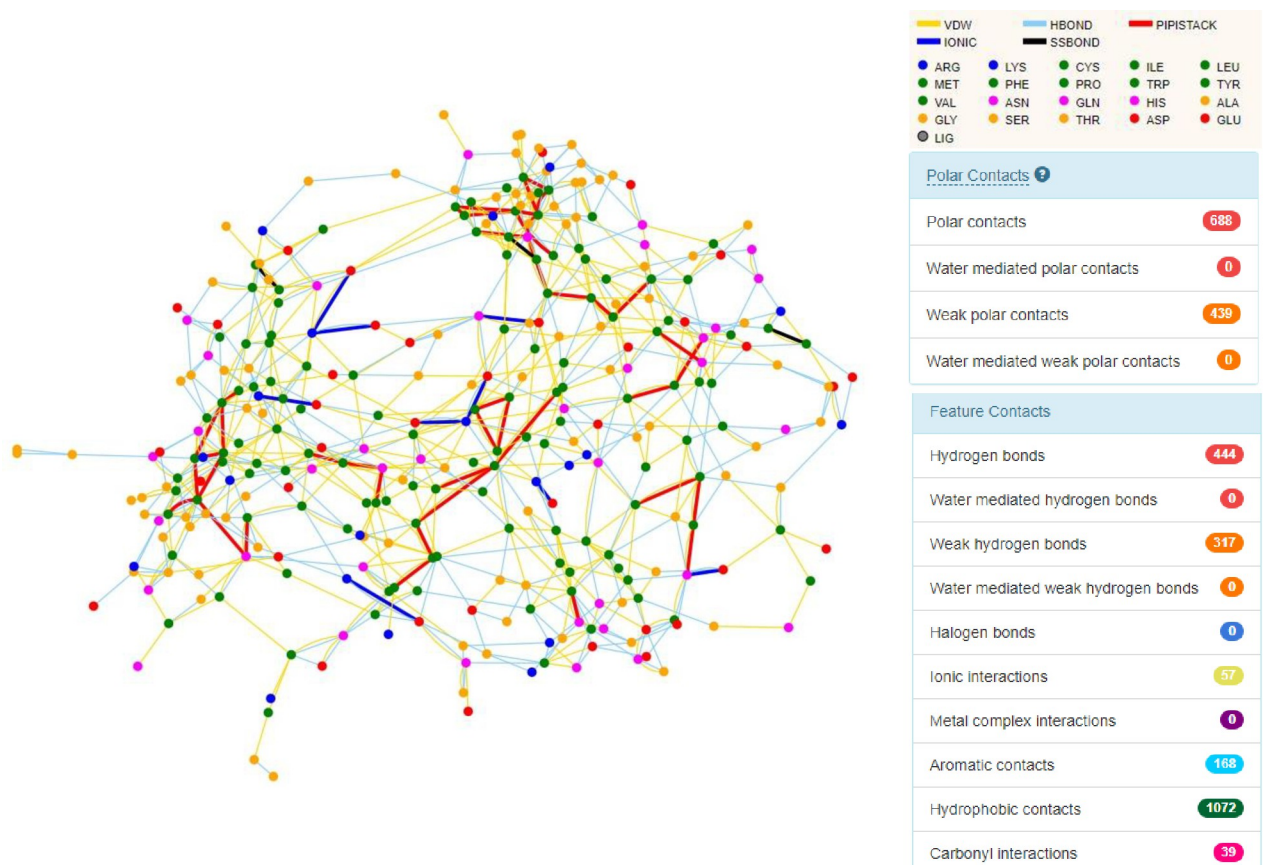


**Fig 3. Intramolecular interaction of  $\beta$ ManAo.** Main interactions are designated as Van der Waals interactions (yellow), conventional H-bonds (light blue), attractive non covalent  $\pi$ - $\pi$  stacking interactions (red), electrostatic attraction as ionic bonds (dark blue) and disulfide bridges (black). Right columns represent the total number of different interactions.  $\beta$ ManAo had majorly hydrogen bonds for the stability of the enzyme with two disulfide bonds at the positions Cys373-Cys324 and Cys312-Cys305.

<https://doi.org/10.1371/journal.pone.0268333.g003>

4-mannanases from *Trichoderma reesei* and *Podospora anserina* had four (Cys26-Cys29, Cys172-Cys175, Cys265-Cys272, and Cys284-Cys334) and three (Cys180-Cys184, Cys272-Cys279, and Cys291-Cys342) disulfide bonds, respectively [45, 46].  $\beta$ ManAo showed several weak interactions which are important for the stabilization of the enzyme as well as in the determination of its tertiary structure. Similarly, salt bridges have a pivotal role in maintaining protein stability and solubility. The amino acids, His/Asp, Lys/Asp, Lys/Glu, Arg/Asp, Arg/Glu, His/Asp and His/Glu are required to form salt bridges. Among the six salt bridges, His/Asp formed 32% of the total salt bridges, which were less than 4.0 Å. Lys/Asp residues formed 25% of the salt bridges, while Arg/Asp and Arg/Glu residues accounted for 12% of the salt bridges each, in the  $\beta$ ManAo structure.

### 3.5 Molecular docking with mannotriose

The interaction between the substrate and enzyme (mannotriose, M3 and  $\beta$ ManAo) was studied by molecular docking with the help of AutoDock 4.2 and visualized by BIOVIA Discovery Studio Visualizer. The list of time dependent specific amino acids of the protein interacting with the mannotriose *via* different bonds is given in S1 Table.  $\beta$ ManAo interacted with M3 *via* five conventional H-bonds. The H-bonded amino acids were Glu208 (2 bonds), Asn151 and Glu244 (2 bonds) (Fig 4A and 4B).

The binding energy for M3 was -5.4 kcal/mol with a  $pK_d$  value of 4.0 and a cluster RMS value of 0.00 Å. The ligand binding efficiency was found to be -0.15.

### 3.6 Molecular dynamics simulation

**3.6.1 Radius of gyration (RG).** The RG value was calculated for investigating the compactness and structural changes in the  $\beta$ ManAo and  $\beta$ ManAo-M3 complexes. The RG value of a protein is calculated by measuring the root mean square distance of an atom of protein in relation with the center of mass of the protein. The overall average RG value of  $\beta$ ManAo was ~1.90 nm and ~1.91 nm in case of  $\beta$ ManAo-M3 complex after 100 ns MD simulations were run (Fig 5A). Both the structures remained intact after 20 ns and throughout the full MD simulation run. The compactness and structural integrity of the  $\beta$ ManAo-M3 complex were similar to the native protein. RMSD value of  $C_{\alpha}$  atoms was also well correlated with the RG value. The

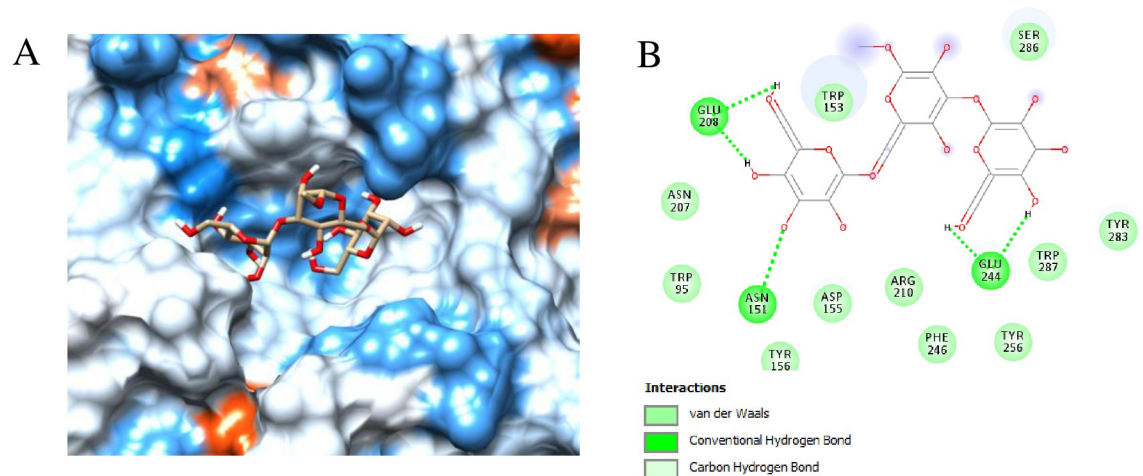


**Fig 4. Binding cavity and the 2D chemical figure of the binding site residues of *A. oryzae*  $\beta$ -mannanase ( $\beta$ ManAo) with mannotriose (M3).** (A) Catalytic cavity of  $\beta$ ManAo, (B) Active site amino acids interacting with M3 after docking.

<https://doi.org/10.1371/journal.pone.0268333.g004>

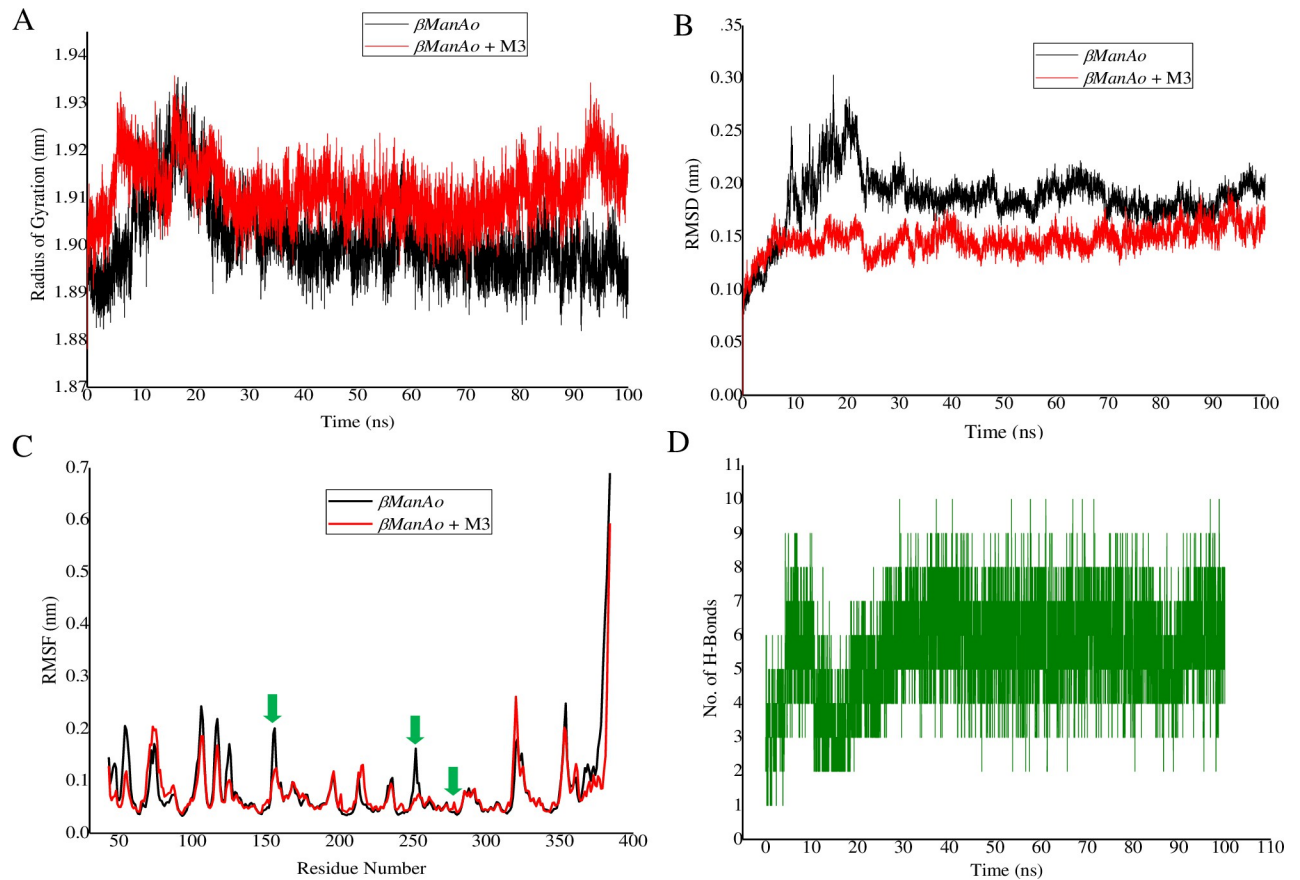


**Fig 5. Analysis of different protein dynamics parameters.** (A) Combined radius of gyration (RG) plot of  $\beta$ ManAo and  $\beta$ ManAo-M3 at 310.15 K, (B) Time dependent backbone RMSD values with respect to the starting structure of protein and protein ligand complex during MD simulations, (C) Combined RMSF plot and (D) Number of total H-bonds interacting with M3 during simulation. Glu208, Glu262 and Asn155 were the main catalytic amino acids involved in H-bonding. Color illustration: Native Protein designated as  $\beta$ ManAo (black) and  $\beta$ ManAo-M3 complex (red).

<https://doi.org/10.1371/journal.pone.0268333.g005>

differences between the two structures were insignificant, which suggested that the  $\beta$ ManAo-M3 complex was stable over the period and that the modeled protein folding was correct.

**3.6.2 Root Mean Square Deviation (RMSD) analysis.** The main motive behind the MD simulation runs was to understand the stability of the protein-ligand complex after docking. The RMSD was calculated for the overall 100 ns simulation run. The RMSD value of a protein provides an insight into the structural conformation through the MD run and the complex RMSD value helps to understand the stability during the catalytic activity of the protein. The RMSD graphs of both  $\beta$ ManAo and  $\beta$ ManAo-M3 were generated with respect to the modeled structure during the 100 ns. The average RMSD value of  $\beta$ ManAo was  $\sim 0.186$  nm, whereas that of the  $\beta$ ManAo-M3 complex was found to be 0.147 nm (Fig 5B). Initially, a light fluctuation in the RMSD value for  $\beta$ ManAo from 10 ns to 25 ns was observed, but it was altogether absent in case of the  $\beta$ ManAo-M3 docked complex. The possible reason behind the  $\beta$ ManAo-M3 stability was the binding of the substrate with the active site amino acid residues located in the structure. Overall, both predicted structures, the  $\beta$ ManAo and the  $\beta$ ManAo-M3 complex, remained stable throughout the 100 ns MD simulation run without any significant variance between them, and most of the residues of the protein had stable conformations as minimum amino acids switched their native conformation from bends to turn. The results suggested that the catalytic residues on interaction with mannotriose displayed stability in the overall run.

**3.6.3 Root Mean Square Fluctuations (RMSF).** The RMSF of each of the 342 residues were determined and superimposed on both  $\beta$ ManAo and the  $\beta$ ManAo-M3 complex (Fig 5C). The average RMSF values of both showed moderate fluctuation from 0.077 to 0.083 nm. Overall, the root-mean-square fluctuation of the active site binding residues (Asp151, Glu244) of the  $\beta$ ManAo-M3 complex were decreased as compared to  $\beta$ ManAo (marked by a green arrow) (Fig 5C). The binding residues position between 200 to 300 amino acid sequence had low RMSF fluctuation between indicating compactness and rigidity of the catalytic cavity. The last ten C-terminal residues showed a highly fluctuating graph, possibly because of the unavailability of modeled protein structure information.

**3.6.4 H-bond interaction.** The H-bond interaction was analyzed for the docked complex of  $\beta$ ManAo-M3 for 100 ns, using a standard GROMACS hbond tool as shown in Fig 5D. Glu244 formed continuous two conventional H-bonds with mannotriose as a major active site residue. The ligand-protein complex was stabilized with an average of six or seven H-bonds in the 100 ns run. In addition, Glu208, Glu262 and Asn155 also participated in H-bonding. Besides these residues, Ser286, Ser285, Arg210 and Trp287 did not form H-bonds, but were found to actively participate by Van der Waals and electrostatic interactions in stabilizing the enzyme-ligand complex.

**3.6.5 Binding pocket dynamics.** The overall dynamics of the protein active site was monitored as a function of the simulation time frame of 100 ns. The  $\beta$ ManAo displayed a flexible active site that varied in volume ranging from  $293 \text{ \AA}^3$  to  $599 \text{ \AA}^3$  (Fig 6) as the M3 molecule moved from the initial (docked) position to probable active site release position (Fig 7A) over the simulation time frame of this study.

The residue Tyr283 acts as an anchor point between the initial and probable substrate release conformational state of M3 (Fig 7B). The comprehensive representation of overall appearing and disappearing pocket is shown in (Fig 7C).

**3.6.6 Principal component analysis (PCA).** PCA was used for analyzing the dynamics of protein and also to understand the dynamic properties in light of the MD simulation run. Two eigenvector projections (PC1 & PC2) for  $\beta$ ManAo and  $\beta$ ManAo-M3 are shown in Fig 8A & 8B.

These principal components showed maximum molecular motion in the protein as a function of distance. In case of  $\beta$ ManAo (PC1), the initial motion was anisotropic. This may be attributed to the high movement with different directions of  $\alpha_8$ -helix present in the C-terminus of the protein [47]. These movements resolved with increasing time and were absent in the case of enzyme-ligand complex, which indicated that mannotriose binding increased the stability of the overall protein structure. The trace values of the two eigenvectors were more negative in the case of  $\beta$ ManAo-M3 complex compared to  $\beta$ ManAo, which led to more flexibility in the  $C_\alpha$  atom. The binding of the mannotriose expanded the protein and changed the overall motion of the protein.

**3.6.7 Free energy landscape (FEL) analysis.** The free energy landscape (FELs) was generated as a function of RMSD and RG values obtained through the MD trajectory. The free energy profiles of  $\beta$ ManAo and  $\beta$ ManAo-M3 complex were similar in nature. In the case of  $\beta$ ManAo, there were multiple local minima and global minima with a Gibbs free energy difference of 5–6 kJ/mol while there was a single global energy minimum for the  $\beta$ ManAo-M3 complex. Therefore, the FEL appeared more funnel-bottom like than the  $\beta$ ManAo-M3 complex (Fig 9A & 9B).

These results led to the conclusion that  $\beta$ ManAo had high conformation sub-states, more complex dynamic behavior and was richer in conformational diversity but binding with mannotriose these characters were subsidized. These results are similar to the previous report by Sang et al. [48], who suggested that a psychrophilic proteinase K had more local energy minima and a funnel-like free energy landscape than a mesophilic proteinase K. The FELs are

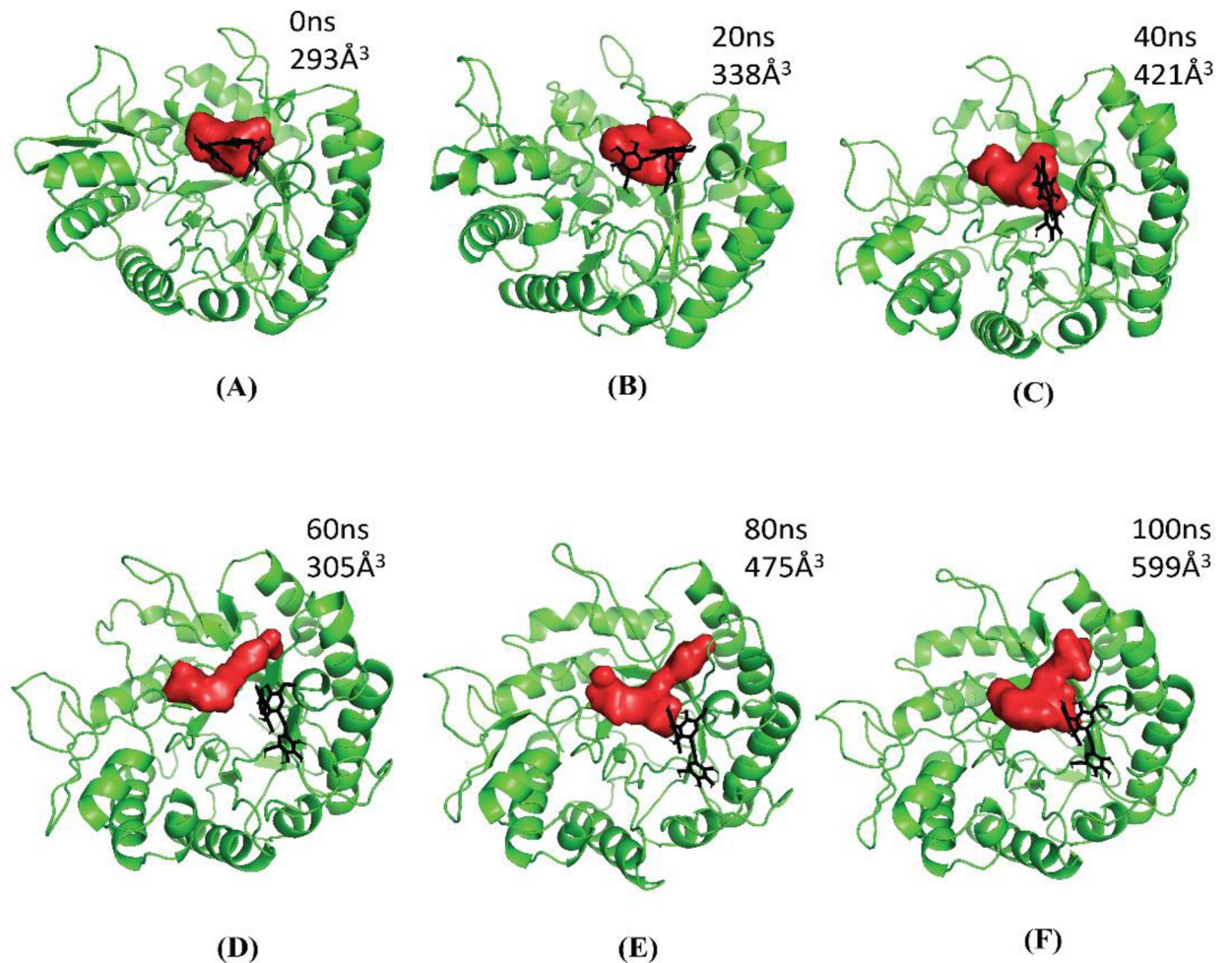


**Fig 6. The flexibility and volume analysis of substrate binding pocket of  $\beta$ ManAo bound with M3.** Corresponding time intervals of (A) 0 ns, (B) 20 ns, (C) 40 ns, (D) 60 ns, (E) 80 ns and (F) 100 ns.

<https://doi.org/10.1371/journal.pone.0268333.g006>

useful in comparing the differences in kinetic and thermodynamic behavior between two forms of proteins.

**3.6.8 Binding energy calculation.** Four different energy components for the ligand mannotriose towards the  $\beta$ ManAo binding affinity were calculated.  $\Delta G_{vdw}$  for the M3 was found to be  $\sim -20$  kcal/mol; whereas the  $\Delta G_{elec}$  value was  $-115$  kcal/mol, which significantly contributed to the binding of the complex (Fig 10A). Comparison of the free energy components indicated that electrostatic energy is the main driving force behind the binding of mannotriose to  $\beta$ ManAo. In general, the complex structure has a low binding free energy ( $\Delta G_{bind} \sim -24$  kcal/mol) and it is relatively stable. Enthalpy of binding ( $\Delta H$ ) indicated the change in energy after binding of the ligand and was calculated as  $\sim -38$  kcal/mol (Fig 10B). The high negative value of binding enthalpy reflected the formation of energetically more favorable non-covalent interactions between  $\beta$ ManAo and mannotriose. The overall  $-T\Delta S$  value was positive, indicating that the entropy of the system is negative, as the degree of freedom of the overall system had decreased. It was concluded that the complex was stable on the basis of heat energy distribution over the overall thermodynamic system. Per-residue energy decomposition in Fig 10C showed that Glu244 had high negative value of free energy contribution and actively participated for binding with M3 over the run. In addition, Ser286, Tyr283, Trp287 and Trp153 also

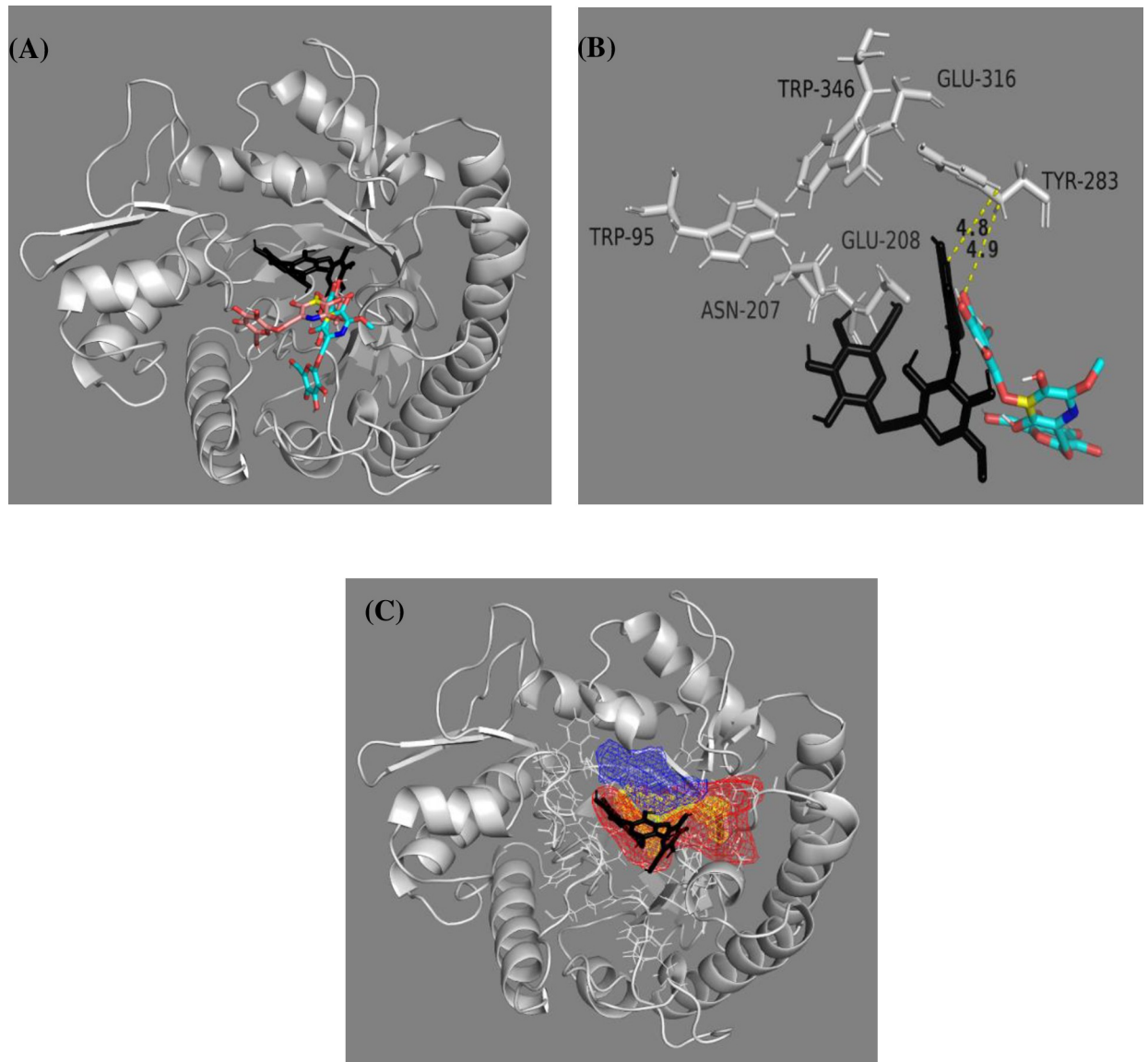


**Fig 7. The overall transition and interaction of M3 with  $\beta$ ManAo.** (A) The transition of M3 from the initial docked position (black) to the final position (cyan) in the binding pocket of  $\beta$ ManAo, (B) the interaction of M3 with the binding site residues (white) and anchored position of initial and final state of M3 with residue Tyr283 showing  $\pi$ - $\pi$  interactions at a distance of 4.8 and 4.9 Å, respectively. In (C), the overall pocket dynamics of  $\beta$ ManAo in complex with M3 is shown. The average pocket over the simulation is marked in yellow, appearing pocket in red, disappearing pocket in blue and M3 in black.

<https://doi.org/10.1371/journal.pone.0268333.g007>

favorable binding. Fig 10D shows the per-residue per frame energy contribution of actively participating amino acids present in the catalytic cavity of  $\beta$ ManAo. All the residues had favorable binding energy, except Glu208 and Arg210, which were binding unfavorably with the mannotriose (red sections in Fig 10D).

**3.6.9 Secondary structure analysis of proteins.** Define Secondary Structure of Proteins (DSSP) analysis elucidated the different secondary structure elements, such as alpha helices, beta sheets, and coils throughout the dynamic simulation. The results suggested that the binding of mannotriose to  $\beta$ ManAo, in particular with Glu244, changed the secondary structure

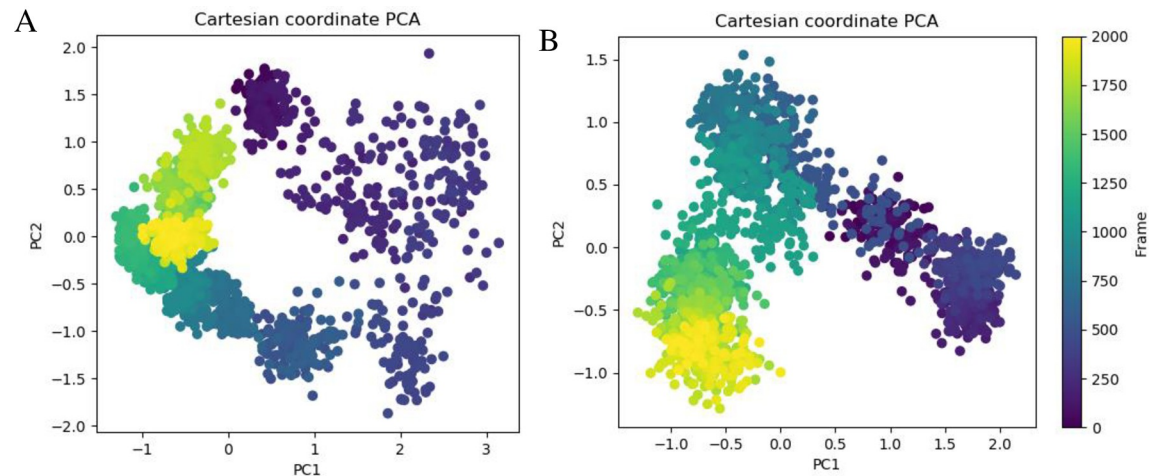


**Fig 8. Principal component analysis (PCA) plot of  $C_{\alpha}$  atoms created by plotting first two eigenvectors in conformational space.** (A) PCA plot of  $\beta$ ManAo and (B) PCA plot of ManAo-M3 complex.

<https://doi.org/10.1371/journal.pone.0268333.g008>

from an alpha helix to turn and vice versa transition between 20 and 60 ns (Fig 11). Interestingly, in case of transition for the Tyr283 containing secondary structure, the transition from alpha helix to turn was constant from about 50 to 100 ns (Fig 11).

The possible reason for this may be help turn the protein to pack the side chain and local environment for more stable conformation. It also yielded strong conformational propensities. The change to  $\beta$ -turn assists the protein to be more surface exposed for suitable interaction with mannotriose [49]. Turn plays a key role in the binding to the ligand and provides thermodynamic stability to the protein. For example, when a central turn in plastocyanin was mutated in a combinatorial fashion, it lost its binding ability towards its metal cofactor [50]. So, the helix-turn transition in the case of the  $\beta$ ManAo-M3 complex favors thermodynamic stability and acts passively in folding the protein [49].

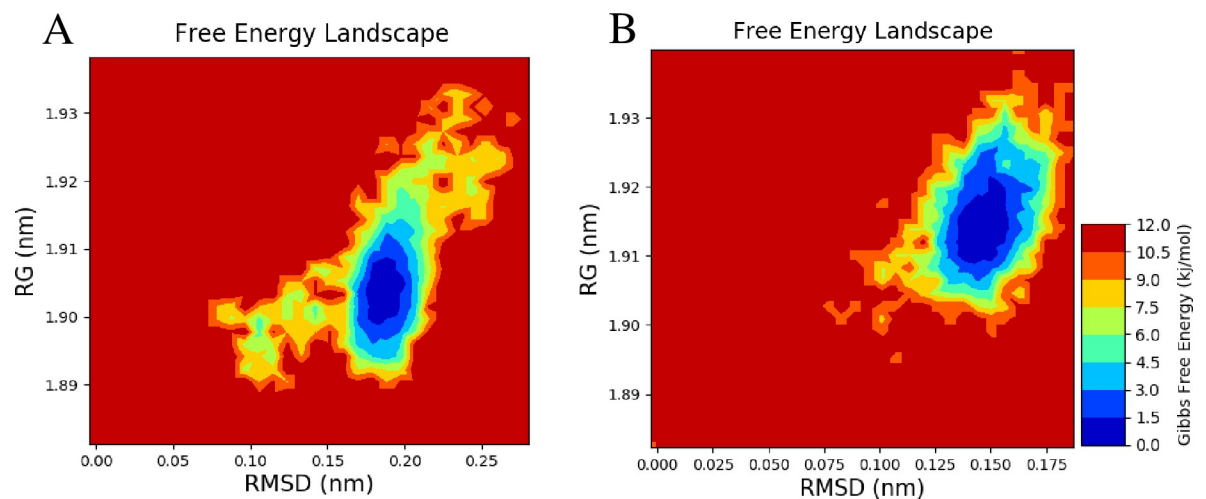


**Fig 9. Contour maps of free energy landscape as a function of RMSD (nm) value and radius of gyration (RG, nm).** (A)  $\beta$ ManAo and (B)  $\beta$ ManAo-M3 complex. The  $\beta$ ManAo-M3 complex had lower subset of energy to reach the favorable state where the only enzyme  $\beta$ ManAo had more than one energy subset.

<https://doi.org/10.1371/journal.pone.0268333.g009>

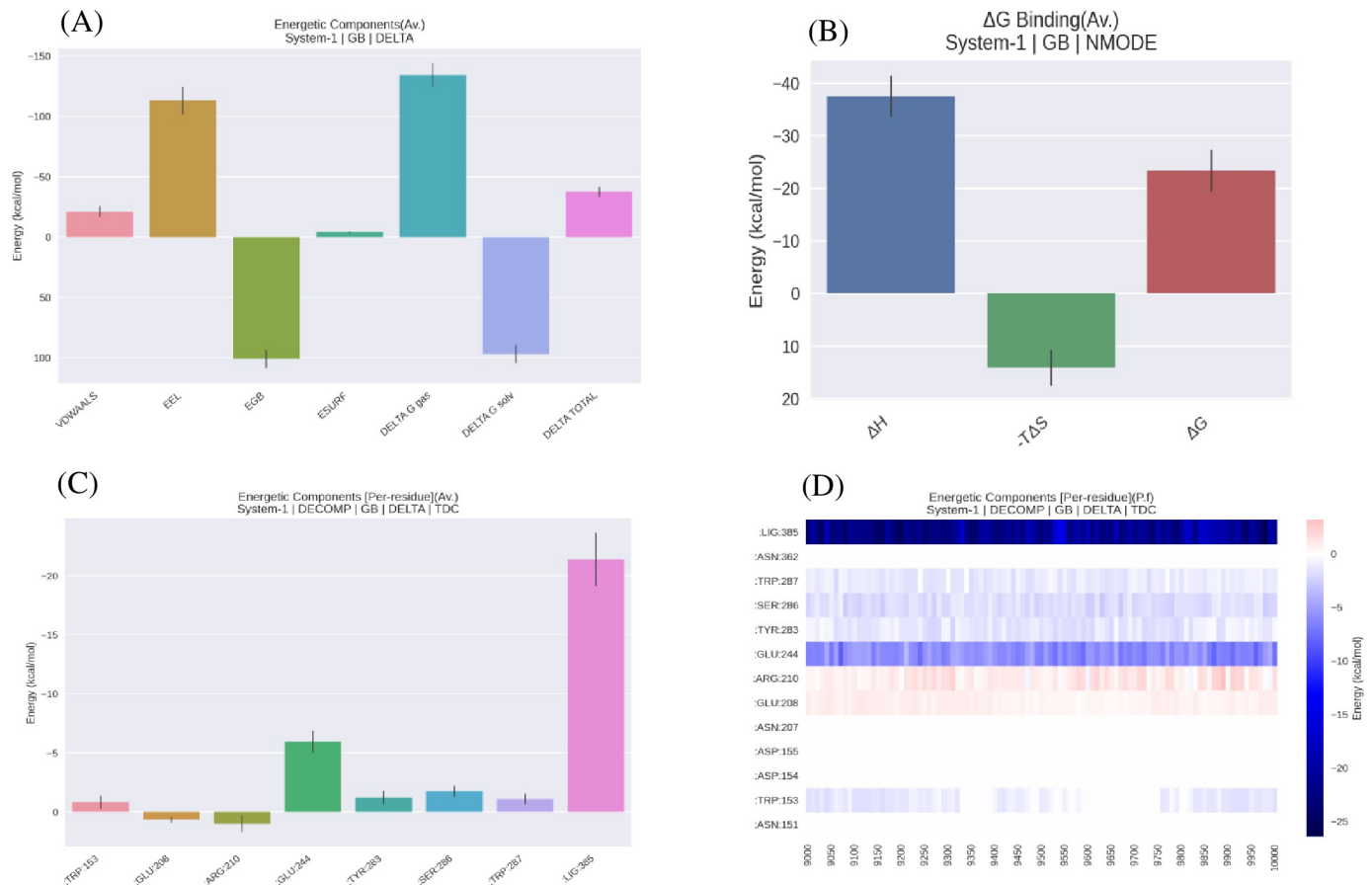


**Fig 10. Binding free energy analysis of  $\beta$ ManAo-M3 complex.** (A) Enthalpic contributions to the  $\beta$ ManAo-M3 interactions, (B) Total binding free energy ( $\Delta G_{\text{bind}}$ ) for  $\beta$ ManAo-M3 complex, (C) Per residue contribution in the binding free energy of M3 with  $\beta$ ManAo, (D) Total decomposition of free energy contribution per residue and per frame of MD stimulation run (90-100ns). LIG385 refers to M3.

<https://doi.org/10.1371/journal.pone.0268333.g010>

## 4. Conclusion

In the present study, the hypothetical model preparation and binding mechanism of *A. oryzae*  $\beta$ -mannanase with mannotriose was reported. All validated scores indicated that the modeled protein was correct for the molecular interaction. Docking analysis revealed that mainly polar amino acids like Glu208 and Glu244 play a key role at the binding site of the enzyme. However, other amino acids, namely Asn207, Asp155 and Ser286, are also important for the binding with the mannotriose. The docking results are validated through MD simulations and MMGBSA calculations, which reveal that the actual Glu244 residue is involved in the main catalytic reaction. The binding pocket of  $\beta$ ManAo displayed a range of flexibility and change in volume to attune with the M3 displacement. From the volume of the substrate binding cavity estimated in this study, it is predicted that the enzyme could accommodate substrate molecules from M3 to M6. Metadynamic analysis showed the thermodynamic characters of protein and the protein ligand complex. Further, a detailed meta-dynamic analysis showed the change in secondary structure from helix to  $\beta$ -turn at the binding site for stabilizing the backbone hydrogen bonds for binding with ligand. Thus, the present study illustrated the structural properties of a prominent mannanase from a commonly explored fungus, which provides insights for improving the enzyme through protein engineering for the efficient degradation of mannans.

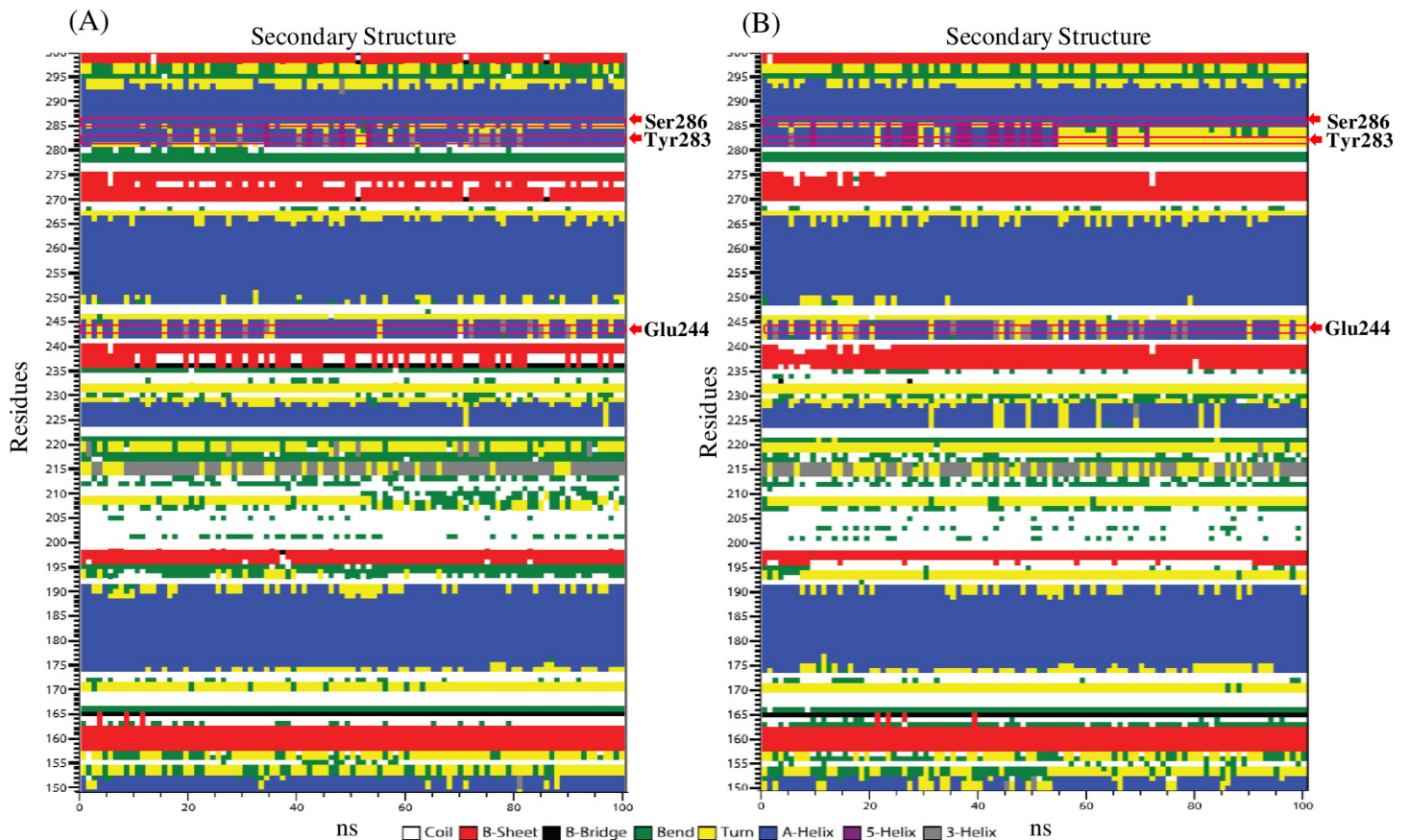


**Fig 11. Residue wise secondary structure of  $\beta$ -mannanase.** (A)  $\beta$ ManAo and (B)  $\beta$ ManAo-M3 during 100 ns dynamic simulation. The secondary structures were labeled as different color and three main binding amino acids over the simulation run (Glu244, Tyr283 and Ser286) were denoted by red arrow. A helix-turn transition was observed in Glu244 and Tyr283 amino acids.

<https://doi.org/10.1371/journal.pone.0268333.g011>

## Supporting information

**S1 Table. Interaction of  $\beta$ ManAo amino acids with substrate (M3) involved in different chemicals bonds.**  
(DOCX)

## Acknowledgments

The infrastructural support of sophisticated instrumentation center and DST-PURSE (II) at Dr. Harisingh Gour Vishwavidyalaya, Sagar, MP, India is duly acknowledged. We would like to thank Rhodes University for APC. Author UKJ acknowledges ICMR, New Delhi for student fellowship.

## Author Contributions

**Conceptualization:** Uttam Kumar Jana, Naveen Kango.

**Data curation:** Uttam Kumar Jana, Gagandeep Singh.

**Formal analysis:** Uttam Kumar Jana, Gagandeep Singh.

**Investigation:** Uttam Kumar Jana, Gagandeep Singh.

**Methodology:** Uttam Kumar Jana, Gagandeep Singh.

**Project administration:** Uttam Kumar Jana, Naveen Kango.

**Resources:** Hemant Soni, Brett Pletschke, Naveen Kango.

**Software:** Uttam Kumar Jana.

**Supervision:** Brett Pletschke, Naveen Kango.

**Validation:** Uttam Kumar Jana, Hemant Soni, Naveen Kango.

**Visualization:** Uttam Kumar Jana, Gagandeep Singh.

**Writing – original draft:** Uttam Kumar Jana.

**Writing – review & editing:** Uttam Kumar Jana, Gagandeep Singh, Hemant Soni, Brett Pletschke, Naveen Kango.

## References

1. Jana UK, Kango N, Pletschke B. Hemicellulose-Derived Oligosaccharides: Emerging Prebiotics in Disease Alleviation. *Front Nutr.* 2021; 8: 1–13. <https://doi.org/10.3389/fnut.2021.670817> PMID: [34386513](https://pubmed.ncbi.nlm.nih.gov/34386513/)
2. Jana UK, Suryawanshi RK, Prajapati BP, Kango N. Prebiotic mannoooligosaccharides: Synthesis, characterization and bioactive properties. *Food Chem.* 2021; 342: 128328. <https://doi.org/10.1016/j.foodchem.2020.128328> PMID: [33257024](https://pubmed.ncbi.nlm.nih.gov/33257024/)
3. Suryawanshi RK, Jana UK, Prajapati BP, Kango N. Immobilization of *Aspergillus quadrilineatus* RSNK-1 multi-enzymatic system for fruit juice treatment and mannoooligosaccharide generation. *Food Chem.* 2019; 289: 95–102. <https://doi.org/10.1016/j.foodchem.2019.03.035> PMID: [30955678](https://pubmed.ncbi.nlm.nih.gov/30955678/)
4. Suryawanshi RK, Kango N. Production of mannoooligosaccharides from various mannans and evaluation of their prebiotic potential. *Food Chem.* 2021; 334: 127428. <https://doi.org/10.1016/j.foodchem.2020.127428> PMID: [32688173](https://pubmed.ncbi.nlm.nih.gov/32688173/)
5. Sakai K, Mochizuki M, Yamada M, Shinzawa Y, Minezawa M, Kimoto S, et al. Biochemical characterization of thermostable  $\beta$ -1,4-mannanase belonging to the glycoside hydrolase family 134 from *Aspergillus oryzae*. *Appl Microbiol Biotech.* 2017; 101: 3237–3245. <https://doi.org/10.1007/s00253-017-8107-x> PMID: [28105485](https://pubmed.ncbi.nlm.nih.gov/28105485/)
6. Rosengren A, Reddy SK, Sjoberg JS, Aurelius O, Logan DT, Kolenova K, et al. An *Aspergillus nidulans*  $\beta$ -mannanase with high transglycosylation capacity revealed through comparative studies within glycosidase family 5. *Appl Microbiol Biotech.* 2014; 98: 10091–10104. <https://doi.org/10.1007/s00253-014-5871-8> PMID: [24950755](https://pubmed.ncbi.nlm.nih.gov/24950755/)
7. Hilge M, Gloor SM, Rypniewski W, Sauer O, Heightman TD, Zimmermann W, et al. High-resolution native and complex structures of thermostable  $\beta$ -mannanase from *Thermomonospora fusca*—Substrate specificity in glycosyl hydrolase family 5. *Structure.* 1998; 6: 1433–1444. [https://doi.org/10.1016/S0969-2126\(98\)00142-7](https://doi.org/10.1016/S0969-2126(98)00142-7)
8. Dhawan S, Kaur J. Microbial mannanases: An overview of production and applications. *Crit Rev Biotechnol.* 2007; 27: 197–216. <https://doi.org/10.1080/07388550701775919> PMID: [18085462](https://pubmed.ncbi.nlm.nih.gov/18085462/)
9. Machida M, Yamada O, Gomi K. Genomics of *Aspergillus oryzae*: learning from the history of koji mold and exploration of its future. *DNA Res.* 2008; 15: 173–183. <https://doi.org/10.1093/dnares/dsn020> PMID: [18820080](https://pubmed.ncbi.nlm.nih.gov/18820080/)
10. Jana UK, Suryawanshi RK, Prajapati BP, Soni H, Kango N. Production optimization and characterization of mannoooligosaccharide generating  $\beta$ -mannanase from *Aspergillus oryzae*. *Bioresour Technol.* 2018; 268: 308–314. <https://doi.org/10.1016/j.biortech.2018.07.143> PMID: [30092484](https://pubmed.ncbi.nlm.nih.gov/30092484/)
11. Jana UK, Kango N. Characteristics and bioactive properties of mannoooligosaccharide derived from agro-waste mannans. *Int J Biol Macromol.* 2020; 149: 931–940. <https://doi.org/10.1016/j.ijbiomac.2020.01.304> PMID: [32014482](https://pubmed.ncbi.nlm.nih.gov/32014482/)
12. Muhammed MT, Aki-Yalcin E. Homology modeling in drug discovery: Overview, current applications, and future perspectives. *Chem Biol Drug Des.* 2019; 93: 12–20. <https://doi.org/10.1111/cbdd.13388> PMID: [30187647](https://pubmed.ncbi.nlm.nih.gov/30187647/)
13. Meng X. Y., Zhang H. X., Mezei M., & Cui M. Molecular docking: a powerful approach for structure-based drug discovery. *Current computer-aided drug design. Curr Comput Aided Drug Des.* 2011; 7: 146–157.

14. Skariyachan S, Khangwal I, Niranjana V, Kango N, Shukla P. Deciphering effectual binding potential of xylo-substrates towards xylose isomerase and xylokinase through molecular docking and molecular dynamic simulation. *J Biomol Struct Dyn*. 2020; 0: 1–10. <https://doi.org/10.1080/07391102.2020.1772882> PMID: 32508225
15. Hospital A, Goni JR, Orozco M, Gelpi JL. Molecular dynamics simulations: Advances and applications. *Adv. Appl. Bioinform. Chem*. 2015; 8: 37–47. <https://doi.org/10.2147/AABC.S70333> PMID: 26604800
16. Schwede T, Kopp J, Guex N, Peitsch MC. SWISS-MODEL: An automated protein homology-modeling server. *Nucleic Acids Res*. 2003; 31: 3381–3385. <https://doi.org/10.1093/nar/gkg520> PMID: 12824332
17. Bhattacharya D, Nowotny J, Cao R, Cheng J. 3Drefine: an interactive web server for efficient protein structure refinement. *Nucleic Acids Res*. 2016; 44: W406–W409. <https://doi.org/10.1093/nar/gkw336> PMID: 27131371
18. Geourjon C, Deleage G. Sopma: Significant improvements in protein secondary structure prediction by consensus prediction from multiple alignments. *Bioinformatics*. 1995; 11: 681–684. <https://doi.org/10.1093/bioinformatics/11.6.681> PMID: 8808585
19. Maiti R, Van Domselaar GH, Zhang H, Wishart DS. SuperPose: A simple server for sophisticated structural superposition. *Nucleic Acids Res*. 2004; 32: 590–594. <https://doi.org/10.1093/nar/gkh477> PMID: 15215457
20. Laskowski RA, MacArthur MW, Moss DS, Thornton JM. PROCHECK: a program to check the stereochemical quality of protein structures. *J Appl Crystallogr*. 1993; 26: 283–291. <https://doi.org/10.1107/s0021889892009944>
21. Wiederstein M, Sippl MJ. ProSA-web: Interactive web service for the recognition of errors in three-dimensional structures of proteins. *Nucleic Acids Res*. 2007; 35: 407–410. <https://doi.org/10.1093/nar/gkm290> PMID: 17517781
22. Colovos C, Yeates TO. Verification of protein structures: Patterns of nonbonded atomic interactions. *Protein Sci*. 1993; 2: 1511–1519. <https://doi.org/10.1002/pro.5560020916> PMID: 8401235
23. Luthy R, Bowie J, Eisenberg D. Verify3D: Assessment of protein models with three-dimensional profiles. *Methods Enzymol*. 1997; 277: 396–404. [https://doi.org/10.1016/s0076-6879\(97\)77022-8](https://doi.org/10.1016/s0076-6879(97)77022-8) PMID: 9379925
24. Heinig M, Frishman D. STRIDE: A web server for secondary structure assignment from known atomic coordinates of proteins. *Nucleic Acids Res*. 2004; 32: 500–502. <https://doi.org/10.1093/nar/gkh429> PMID: 15215436
25. Benkert P, Biasini M, Schwede T. Toward the estimation of the absolute quality of individual protein structure models. *Bioinformatics*. 2011; 27: 343–350. <https://doi.org/10.1093/bioinformatics/btq662> PMID: 21134891
26. Jubb HC, Higuero AP, Ochoa-Montano B, Pitt WR, Ascher DB, Blundell TL. Arpeggio: a web server for calculating and visualising interatomic interactions in protein structures. *J Mol Biol*. 2017; 429: 365–371. <https://doi.org/10.1016/j.jmb.2016.12.004> PMID: 27964945
27. Piovesan D, Minervini G, Tosatto SCE. The RING 2.0 web server for high quality residue interaction networks. *Nucleic Acids Res*. 2016; 44: W367–W374. <https://doi.org/10.1093/nar/gkw315> PMID: 27198219
28. Kumar S, Nussinov R. Salt bridge stability in monomeric proteins 1 Edited by J. M. Thornton. *J Mol Biol*. 1999; 293: 1241–1255. <https://doi.org/10.1006/jmbi.1999.3218> PMID: 10547298
29. Tian W, Chen C, Lei X, Zhao J, Liang J. CASTp 3.0: Computed atlas of surface topography of proteins. *Nucleic Acids Res*. 2018; 46: W363–W367. <https://doi.org/10.1093/nar/gky473> PMID: 29860391
30. Trott O, Olson AJ. AutoDock Vina: Improving the speed and accuracy of docking with a new scoring function, efficient optimization, and multithreading. *J Comput Chem*. 2009; 31: 455–461. <https://doi.org/10.1002/jcc.21334> PMID: 19499576
31. Jimenez J, Skalic M, Martinez-Rosell G, De Fabritiis G. KDEEP: Protein-ligand absolute binding affinity prediction via 3D-convolutional neural networks. *J Chem Inf Model*. 2018; 58: 287–296. <https://doi.org/10.1021/acs.jcim.7b00650> PMID: 29309725
32. Kagami LP, das Neves GM, da Silva AWS, Caceres RA, Kawano DF, Eifler-Lima VL. LiGRO: a graphical user interface for protein–ligand molecular dynamics. *J Mol Model*. 2017; 23: 5–10. <https://doi.org/10.1007/s00894-017-3475-9> PMID: 28980073
33. Abraham MJ, Murtola T, Schulz R, Pall S, Smith JC, Hess B, et al. Gromacs: High performance molecular simulations through multi-level parallelism from laptops to supercomputers. *SoftwareX*. 2015; 1–2: 19–25. <https://doi.org/10.1016/j.softx.2015.06.001>
34. Sousa Da Silva AW, Vranken WF. ACPYPE—AnteChamber PYthon Parser interfacE. *BMC Res Notes*. 2012; 5: 1–8. <https://doi.org/10.1186/1756-0500-5-367> PMID: 22824207

35. Stank A, Kokh DB, Horn M, Sizikova E, Neil R, Panecka J, et al. TRAPP webserver: Predicting protein binding site flexibility and detecting transient binding pockets. *Nucleic Acids Res.* 2017; 45: W325–W330. <https://doi.org/10.1093/nar/gkx277> PMID: 28431137
36. Kagami LP, das Neves GM, Timmers LFSM, Caceres RA, Eifler-Lima VL. Geo-Measures: A PyMOL plugin for protein structure ensembles analysis. *Comput Biol Chem.* 2020;87. <https://doi.org/10.1016/j.compbiolchem.2020.107322> PMID: 32604028
37. Mario S. Valdes Tresanco, Mario E. Valdes-Tresanco, Pedro A. Valiente & EMF. gmx\_MMPBSA (Version v1.4.3). Zenodo. 2021. <https://doi.org/10.5281/zenodo.4569307>
38. Carter P, Andersen CAF, Rost B. DSSPcont: Continuous secondary structure assignments for proteins. *Nucleic Acids Res.* 2003; 31: 3293–3295. <https://doi.org/10.1093/nar/gkg626> PMID: 12824310
39. Wiedemann C, Kumar A, Lang A, Ohlenschlager O. Cysteines and disulfide bonds as structure-forming units: insights from different domains of life and the potential for characterization by NMR. *Front Chem.* 2020; 8: 1–8. <https://doi.org/10.3389/fchem.2020.00280> PMID: 32391319
40. Sobri MFM, Abd-Aziz S, Bakar FDA, Ramli N. In-silico characterization of glycosyl hydrolase family 1  $\beta$ -glucosidase from *Trichoderma asperellum* UPM1. *Int J Mol Sci* 2020;21. <https://doi.org/10.3390/ijms21114035> PMID: 32512945
41. Pace CN, Fu H, Fryar KL, Landua J, Trevino SR, Schell D, et al. Contribution of hydrogen bonds to protein stability. *Protein Sci.* 2014; 23: 652–661. <https://doi.org/10.1002/pro.2449> PMID: 24591301
42. Takano K, Yamagata Y, Funahashi J, Hioki Y, Kuramitsu S, Yutani K. Contribution of intra- and intermolecular hydrogen bonds to the conformational stability of human lysozyme. *Biochemistry.* 1999; 38: 12698–12708. <https://doi.org/10.1021/bi9910169> PMID: 10504240
43. Wang Y, Azhar S, Gandini R, Divne C, Ezcurra I, Aspeborg H. Biochemical characterization of the novel endo- $\beta$ -mannanase AtMan5-2 from *Arabidopsis thaliana*. *Plant Sci.* 2015; 241: 151–163. <https://doi.org/10.1016/j.plantsci.2015.10.002> PMID: 26706067
44. Rudakiya DM, Patel SH, Narra M. Structural insight into the fungal  $\beta$ -glucosidases and their interactions with organics. *Int J Biol Macromol.* 2019; 138: 1019–1028. <https://doi.org/10.1016/j.ijbiomac.2019.07.177> PMID: 31356936
45. Sabini E, Schubert H, Murshudov G, Wilson KS, Siika-Aho M, Penttila M. The three-dimensional structure of a *Trichoderma reesei*  $\beta$ -mannanase from glycoside hydrolase family 5. *Acta Crystallogr D: Biological Crystallography.* 2000; 56: 3–13. <https://doi.org/10.1107/S0907444999013943> PMID: 10666621
46. Couturier M, Roussel A, Rosengren A, Leone P, Stålbbrand H, Berrin JG. Structural and biochemical analyses of glycoside hydrolase families 5 and 26  $\beta$ -(1,4)-mannanases from *Podospora anserina* reveal differences upon manno-oligosaccharide catalysis. *J Biol Chem.* 2013; 288: 14624–14635. <https://doi.org/10.1074/jbc.M113.459438> PMID: 23558681
47. Das A, Mukhopadhyay C. Application of principal component analysis in protein unfolding: An all-atom molecular dynamics simulation study. *J Chem Phys.* 2007;127. <https://doi.org/10.1063/1.2796165> PMID: 17979396
48. Sang P, Yang LQ, Ji XL, Fu YX, Liu SQ. Insight Derived from molecular dynamics simulations into molecular motions, thermodynamics and kinetics of HIV-1 gp120. *PLoS ONE.* 2014; 9. <https://doi.org/10.1371/journal.pone.0104714> PMID: 25105502
49. Marcelino AMC, Gierasch LM. Roles of  $\beta$ -turns in protein folding: From peptide models to protein engineering. *Biopolymers.* 2008; 89: 380–391. <https://doi.org/10.1002/bip.20960> PMID: 18275088
50. Ybe JA, Hecht MH. Sequence replacements in the central  $\beta$ -turn of plastocyanin. *Protein Sci.* 1996; 5: 814–824. <https://doi.org/10.1002/pro.5560050503> PMID: 8732753